Particuology 115 (2026) 15–24

Contents lists available at ScienceDirect

Particuology

journal homepage: www.elsevier.com/locate/partic

Surface-engineered magnetic nanoparticles with carboxymethyl inulin coating for interface-controlled mineral scale inhibition

Abdelrahman T. Abdelaal[a], Farah M. El-Makaty[b], Malcolm A. Kelland[a], Mohamed F. Mady[b,*]

[a] Department of Chemistry, Bioscience and Environmental Engineering, Faculty of Science and Technology, University of Stavanger, Stavanger, N-4036, Norway
[b] Department of Chemistry and Earth Sciences, College of Arts and Sciences, Qatar University, P.O. Box 2713, Doha, Qatar

HIGHLIGHTS

- Recyclable Fe_3O_4@CMI magnetic nanoparticles developed as scale inhibitors.
- Complete gypsum inhibition achieved at 1–5 ppm under static and HPHT conditions.
- CMI coating preserves magnetite structure and superparamagnetic behavior.
- Scale inhibition governed by interface-controlled disruption of crystal growth.
- Enhanced calcium compatibility enables stable performance in saline brines.

GRAPHICAL ABSTRACT

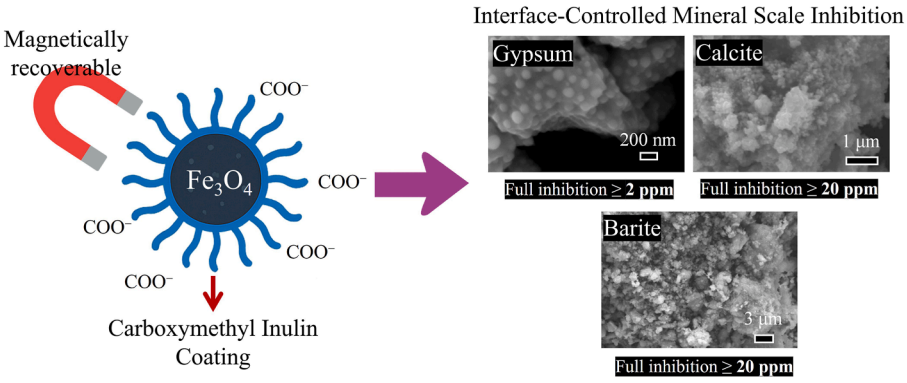

ARTICLE INFO

Keywords:
Magnetic nanoparticles
Carboxymethyl inulin
Scale inhibition
Recycling
Oilfield management

ABSTRACT

In this study, magnetite nanoparticles (Fe_3O_4) were surface-engineered with a biobased carboxymethyl inulin (CMI) coating to develop a recyclable inhibitor for controlling mineral scale formation through interfacial interactions. The Fe_3O_4@CMI nanocomposite was synthesized via co-precipitation, achieving a uniform ~59 wt% polymer layer without altering the cubic spinel structure of magnetite. Comprehensive surface and interface characterization by XRD, FTIR, TGA, VSM, and SEM confirmed the preservation of superparamagnetic properties and effective polymer anchoring via carboxylate–iron interactions. The coated nanoparticles exhibited strong affinity for scaling ions, disrupting crystal nucleation and growth at the solid–liquid interface, as evidenced by morphological transformations of gypsum, calcite, and barite deposits. Under both static and high-pressure-high-temperature dynamic conditions, Fe_3O_4@CMI achieved complete gypsum inhibition at concentrations as low as 1–5 ppm and maintained full efficiency over multiple magnetic recovery cycles. Enhanced calcium compatibility in saline brines further underscores the stability of the modified surface, preventing secondary precipitation and enabling reliable reuse. These results highlight the critical role of interface engineering in tailoring nanoparticle–scale crystal interactions for sustainable and low-discharge chemicals for oilfield scale management.

* Corresponding author.
E-mail address: mmady@qu.edu.qa (M.F. Mady).

https://doi.org/10.1016/j.partic.2026.05.004
Received 16 February 2026; Received in revised form 16 April 2026; Accepted 2 May 2026
Available online 16 May 2026

1. Introduction

The formation of inorganic scale is a widespread issue in industry, particularly in oil and gas production, where it poses serious operational and economic challenges. In subsurface environments, mineral scales form when dissolved salts precipitate and deposit onto internal surfaces, creating complex crystalline layers that restrict fluid flow, narrow tubing diameters, and increase surface roughness. These deposits typically result from shifts in temperature, pressure, pH, or ion saturation. In many cases, scale formation is triggered by the mixing of incompatible waters (formation water and injection water). A common example occurs when sulfate-rich injection water interacts with formation water containing barium (Ba^{2+}), calcium (Ca^{2+}), or strontium (Sr^{2+}), leading to the formation of scales such as barite ($BaSO_4$), celestite ($SrSO_4$), or gypsum ($CaSO_4{\cdot}2H_2O$) (Chauhan et al., 2015; Kodel et al., 2012). In contrast, carbonate scales such as calcite ($CaCO_3$) normally form independently of water mixing. They result from changes in pressure and temperature in the formation water (rich in both carbonate and calcium ions), which shift the carbonate equilibrium, reduce CO_2 solubility, and promote $CaCO_3$ precipitation (Kelland, 2016).

A combination of mechanical and chemical strategies is typically employed to manage scale formation in oilfields, with chemical treatment, particularly the use of scale inhibitors (SIs), being the most widely adopted approach (Kamal et al., 2018; Mady et al., 2022). Scale inhibitors are low-dosage, water-soluble compounds that suppress mineral scales formation, growth, and precipitation in actively producing wells. Their performance depends on various factors, including pH, temperature, the concentration of divalent cations, and the presence of other oilfield chemicals such as corrosion and hydrate inhibitors (Mady et al., 2022).

SIs work by interfering with the scale formation process through three primary mechanisms: nucleation inhibition, crystal growth inhibition, and particle dispersion. Nucleation inhibition, typically achieved by polymeric inhibitors, prevents the initial formation of scale nuclei by lowering the energy barrier for nucleation. Crystal growth inhibition, commonly associated with small molecules such as amino phosphonates, slows or halts the enlargement of existing scale crystals. Dispersion involves stabilizing scale particles in suspension, preventing their aggregation and deposition on surfaces. Although SIs do not dissolve pre-formed scale, they can adsorb onto existing deposits and help suppress further growth (Al-Roomi & Hussain, 2016; Jafar Mazumder, 2020; Kelland, 2016).

Commercially, SIs are classified into two main categories: polymeric types (e.g., polycarboxylates, polysulfonates, and their copolymers) and non-polymeric phosphonates (Frenier and Ziauddin; Popov et al., 2016). These are typically dosed at concentrations ranging from 1 to 50 ppm (Kumar et al., 2018; Liu et al., 2012; Mpelwa & Tang, 2019). While effective, there is an increasing demand for environmentally sustainable alternatives. Biobased compounds such as chitosan (Guo et al., 2012), gallic acid (Boumagoura et al., 2021), and cellulose derivatives (Wang et al., 2020) have been explored for this purpose, though many suffer from poor thermal stability, limiting their effectiveness at elevated oilfield temperatures (Hasson et al., 2011). Nonetheless, polymers such as polyepoxysuccinic acid (PESA) (Wei et al., 2022) and polyaspartic acid (PASP) (Chen et al., 2020; Mady et al., 2021; Zhang et al., 2018) have gained commercial interest, particularly in applications subject to strict environmental regulations.

Polysaccharides are natural polymeric carbohydrates composed of repeating sugar units linked by glycosidic bonds. Their non-toxic, biodegradable, and renewable nature, coupled with a minimal carbon footprint, makes them attractive candidates for sustainable applications (Johannsen, 2003). In addition to their low aquatic toxicity, polysaccharides do not contain phosphorus or nitrogen, which are known to contribute to eutrophication in nutrient-rich environments. Among these natural polymers, inulin is a linear, polydisperse fructan obtained from the roots of chicory plants and has been chemically modified through carboxymethylation to produce carboxymethyl inulin (CMI). This derivative has found utility in oilfield operations (Boels & Witkamp, 2011), drug delivery systems (Santiago-Rodríguez et al., 2013), and as a crystal growth inhibitor in other industrial contexts (Kirboga & Öner, 2013). Polysaccharides have proven effective as stabilizers for iron oxide nano- and microparticles by introducing carboxyl groups into the inulin structure coated on the particles (Dias et al., 2011).

Magnetite nanoparticles (MNPs, Fe_3O_4) have garnered significant interest due to their unique physical properties and versatility in technological applications (Lu et al., 2007; Salman et al., 2021, 2026). These include high-density magnetic storage, sensors, catalysis, and biomedical uses such as targeted drug delivery and imaging (Cornell & Schwertmann, 2003; Cullity, 1972; F Hasany et al., 2013; Häfeli et al., 2013). Their multifunctionality arises from characteristics such as polymorphism (it can exist in different crystal structures despite having the same chemical formula (Fe_3O_4)), variable oxidation states, and phase transitions at the nanoscale. However, MNPs tend to exhibit poor colloidal stability in aqueous media because of their high surface area and strong van der Waals and magnetic interactions. To address this limitation, various surface modification strategies have been explored using stabilizers such as polyethylene glycol (PEG), polyanhydrides, poly (lactic acid), and poly (vinyl alcohol) (PVA) (Wu et al., 2008).

In this study, we present the development of a class of recyclable scale inhibitors based on magnetite nanoparticles coated with carboxymethyl inulin (CMI). This hybrid material combines the magnetic recoverability of MNPs with the biodegradability and scale-inhibiting functionality of CMI. The resulting nanoparticles enable a recyclable treatment approach, where the scale inhibitor SI can be magnetically separated and reused after application. The inhibition performance of the synthesized nanocomposite Fe_3O_4@CMI was evaluated against three common scale types: gypsum, calcite, and barite, in which the supersaturation conditions for the latter two scales were based on the Heidrun oilfield, Norway. This gave the project industrial relevance, representing challenging scaling conditions in an offshore production environment.

2. Experimental

2.1. Chemicals and materials

Iron (III) chloride hexahydrate ($FeCl_3{\cdot}6H_2O$) and iron (II) chloride tetrahydrate ($FeCl_2{\cdot}4H_2O$) were purchased from Acros Organics and Alfa Aesar, respectively. Ammonium hydroxide solution (25%) and carboxymethyl inulin (CMI) were obtained from Sigma-Aldrich. All reagents were of analytical grade with purities of up to 99.9% and were used without further purification. Deionized water (resistivity $\leq$18 MΩ cm^{-1}) was supplied by a Milli-Q purification system.

2.2. Synthesis of magnetic Fe_3O_4 nanoparticles

Following the co-precipitation method (Abdelaal et al., 2024), a total of 51 mmol of $FeCl_3{\cdot}6H_2O$ and 25.9 mmol of $FeCl_2{\cdot}4H_2O$ (in a 2:1 M ratio) were dissolved in 400 mL of degassed deionized water (resistivity $\leq$18 MΩ cm^{-1}) in a three-neck glass flask. The solution was stirred under a nitrogen atmosphere for 30 min at room temperature. Ammonium hydroxide solution (25%) was then added dropwise until the pH reached 10–11, during which the solution colour shifted from red-orange to black, indicating the formation of magnetite precipitate (Fig. 1). The reaction mixture was maintained at room temperature for an additional hour. The resulting black precipitate was collected using a strong magnet and washed multiple times with a 1:1 mixture of Milli-Q water and ethanol.

2.3. Synthesis of Fe_3O_4@CMI nanoparticles

A total of 12.95 mmol of MNPs were redispersed in 200 mL of deionized water, and the pH was adjusted to 12–13. Separately,

30.5 mmol of CMI was dissolved in 200 mL of deionized water and adjusted to pH = 6. The CMI solution was then added to the MNPs dispersion, and the pH of the combined mixture was adjusted to 7. The mixture was sonicated vigorously for 30 min, during which the colour changed from light brown to dark brown, indicating successful interaction. The solution was subsequently stirred on a hot plate at 75–85 °C for 1 h. The resulting precipitate was separated using a strong magnet, washed thoroughly with deionized water and acetone, and concentrated using a rotary evaporator. The final Fe_3O_4@CMI nanocomposite was collected for further characterization.

2.4. Characterization of Fe_3O_4@CMI nanoparticles

The phase purity of Fe_3O_4@CMI was confirmed using X-ray diffraction (XRD, Bruker D8 Advance) with CuKα radiation (λ = 1.5406 Å), operating at 45 kV and 30 mA over a 2θ range of 10°–80° for 40 min. Transmission electron microscopy (TEM, Tecnai G2 FEG 200 kV, FEI) was employed to examine the microstructural features and particle size. TEM samples were prepared by sonicating the powders in isopropyl alcohol for 20 min in an ultrasonicator bath, followed by drop-casting onto 300-mesh carbon-film-coated copper grids. The presence and extent of the polymer coating were examined by Fourier Transform Infrared (FT-IR) spectroscopy (Cary 630, Agilent) over the range of 400–4000 cm^{-1} and quantified by Thermogravimetric Analysis (TGA, Mettler Toledo TGA/DSC 3+) from 25 to 650 °C. Magnetic properties were assessed at 300 K using a Vibrating Sample Magnetometer (VSM, Lake Shore Model 7410) under an applied magnetic field up to 2 T, to confirm their suitability for magnetic recovery and environmental applications after coating.

2.5. Scale inhibition tests

The scale inhibition efficiency of Fe_3O_4@CMI was assessed against three common oilfield scales: gypsum ($CaSO_4{\cdot}2H_2O$), calcite ($CaCO_3$), and barite ($BaSO_4$). The evaluation was carried out using both static jar tests and high-pressure dynamic tube blocking experiments. In each case, the performance of Fe_3O_4@CMI was compared with that of pure CMI.

Synthetic brines were prepared to mimic the chemistry of formation and injection waters typically encountered in oilfield operations. One brine contained scaling cations (e.g., Ca^{2+}, Ba^{2+}), while the other provided scaling anions (CO_3^{2-}, SO_4^{2-}). The scale inhibition tests followed the NACE Standard TM0374-2007 protocol, using brine compositions detailed in previous studies and presented in Table S1 (Mady et al., 2023; Oshchepkov et al., 2020; TM, 2007).

For sulfate scales such as gypsum and barite, scale formation was induced by mixing the two brines under controlled temperature, pressure, and pH to simulate near-wellbore conditions. Although calcite scaling in the field typically results from pressure and temperature drops that shift the carbonate equilibrium in formation water, it was modelled in this study by mixing Ca^{2+} and CO_3^{2-} containing brines to achieve supersaturation and induce precipitation under static and dynamic lab conditions.

Fe_3O_4@CMI stock solutions were prepared at 1000 ppm in deionized water and adjusted to pH 4.5–6 to resemble reservoir conditions. Static tests were performed for gypsum and calcite to assess inhibition under stagnant conditions. Dynamic tube blocking tests were conducted for gypsum, calcite, and barite to evaluate inhibitor performance under flowing, high-pressure conditions.

Following inhibition tests, the morphology of scale deposits was examined using scanning electron microscopy (SEM, Zeiss Supra 35VP) to visualize structural changes induced by the inhibitor.

2.5.1. Static jar scale inhibition testing

To assess the scale inhibition efficiency of Fe_3O_4@CMI under stagnant conditions, static jar tests were conducted against gypsum and calcite scales. A 1:1 mixture of synthetic cationic brine (B1) and anionic brine (B2) was prepared in 50 mL Schott Duran® glass bottles. The scale inhibitor (SI) was prepared separately in deionized water as a stock solution (1000 ppm) and added as a third solution to the system at the desired concentrations (100, 50, 20, 10, 5, 2, and 1 ppm), as shown in Table S2. Two blank samples were also prepared for control measurements.

All samples were thoroughly mixed, sealed, and incubated at 80 °C for 5 h to simulate oilfield reservoir conditions. After incubation, the remaining calcium ion (Ca^{2+}) concentration was measured by complexometric titration using 0.01 M EDTA. For gypsum, ammonium purpurate (murexide) was used as the indicator, while fluorexon (calcein) was used for calcite. Titration was performed by diluting 1 mL of the sample with 49 mL of deionized water, followed by the addition of 200 μL of indicator and pH adjustment to 12–13 using 50% NaOH. The titration endpoint was identified by a colour change from pink to purple, using a Hirschmann™ 25 mL glass burette and a VWR® lab disc stirrer. Each sample was titrated in triplicate to ensure reproducibility, yielding a standard deviation below 5%.

The calcium concentration in ppm was calculated using the following equation:

$$Ca^{2+}(ppm) = \frac{A \times B}{D} \times 40100 \quad (1)$$

where A is the EDTA volume (mL), B is the EDTA concentration (mol/L), D is the sample volume (50 mL), and 40100 is the molecular mass of Ca^{2+} expressed in mDa (millidaltons).

The scale inhibition efficiency was then determined using:

$$\%\ inhibition = \frac{C_a - C_b}{C_o - C_b} \times 100 \quad (2)$$

where C_a is the Ca^{2+} concentration in the test sample, C_b is the concentration in the blank after 5 h, and C_o is the concentration before precipitation. This methodology conforms to the NACE Standard TM0374-2007 (Oshchepkov et al., 2020; Tm, 2007).

2.5.2. Reusability of Fe_3O_4@CMI

The reusability of Fe_3O_4@CMI nanoparticles was evaluated using repeated static inhibition cycles at a concentration of 100 ppm. After

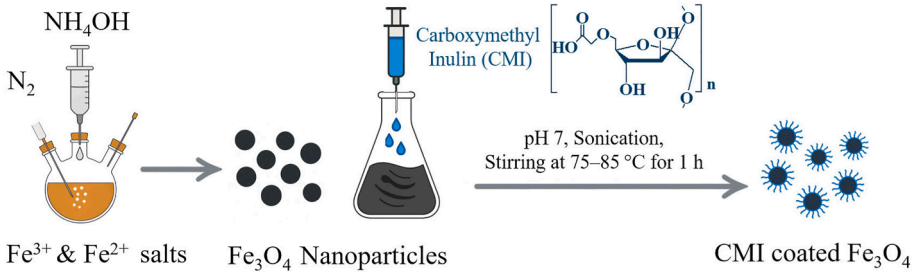

Fig. 1. Schematic representation of the synthesis of CMI-coated Fe_3O_4 nanoparticles.

each experiment, the nanoparticles were recovered using a strong external permanent magnet, allowing efficient separation from the solution. The particles were allowed to fully collect under the magnetic field, and the supernatant was carefully decanted.

The recovered nanoparticles were washed with deionized water to remove residual salts and loosely bound ions, followed by redispersion in fresh deionized water prior to reuse. No additional Fe_3O_4@CMI was added between cycles, and the same recovered material was used for subsequent inhibition experiments.

Any variation in inhibition efficiency over cycles was attributed to possible material loss or surface deactivation during reuse. Although minor loss due to adsorption on scale surfaces cannot be excluded, the consistently high inhibition efficiency suggests minimal loss of active material.

2.5.3. Dynamic tube blocking scale inhibition testing

Dynamic scale inhibition performance was evaluated using the Scale Rig 4000 system (Fig. S1), following the NACE TM31105-2005 standard (capillary precipitation test), to simulate realistic oilfield conditions and assess the failure inhibitor concentration (FIC): the concentration at which rapid scale formation begins when the inhibitor concentration is gradually decreased in the test. The experiments were conducted at a constant temperature of 100 °C, pressure of 1000 psi, and pH between 4 and 6 to assess the effectiveness of Fe_3O_4@CMI as a scale inhibitor under dynamic flow conditions.

During each test, synthetic brines containing scaling ions were injected simultaneously in a 1:1 volumetric ratio using HPLC pumps into a 1.5 m stainless steel capillary tube with an internal diameter of 0.5 mm. The flow rate was maintained at 10 mL/min. The formation of scale was monitored by recording the differential pressure across the capillary as a function of time; an increase in pressure indicated the onset of scale deposition and potential blockage.

Fe_3O_4@CMI was considered effective when the pressure differential remained stable at approximately 2–3 psi for at least 60 min, which is at least three times longer than the scale formation time observed in the blank test. When inhibitors were absent, significant pressure increases occurred rapidly due to scale accumulation. After each experiment, the system was flushed with deionized water followed by a Na_4EDTA cleaning solution for 10 min to dissolve any residual deposits, ensuring the system was reset to its baseline pressure range of 2–3 psi before the next run.

The entire setup utilized a 316 stainless steel micro-bore coil, and flow was maintained with three integrated pumps. Real-time pressure monitoring provided continuous insight into the inhibitor's performance under high-temperature, high-pressure (HTHP) conditions.

2.6. Calcium compatibility

Calcium compatibility tests were performed to evaluate the stability of Fe_3O_4@CMI in the presence of calcium ions under simulated field conditions. These tests aimed to ensure that the coated magnetite scale inhibitor does not form unwanted precipitates when mixed with high-salinity brines, thereby preventing formation damage or operational issues during oilfield application (Mady et al., 2020).

In the test setup, 20 mL of deionized water was added to 50 mL Schott Duran® glass bottles containing Fe_3O_4@CMI at three different concentrations: 100, 1000, and 10,000 ppm. Calcium ions were introduced at concentrations ranging from 100 to 10,000 ppm, along with 30,000 ppm of sodium chloride (3.0 wt%) to mimic brine salinity. The pH of each solution was adjusted to between 4.0 and 4.5, and the mixtures were shaken to ensure homogeneity. The prepared solutions were incubated at 80 °C for 24 h. Visual observations were made at multiple time intervals, 30 min, 1 h, 4 h, and 24 h, to detect any signs of turbidity or precipitation that would indicate incompatibility.

3. Results and discussion

3.1. Physical and magnetic properties

3.1.1. X-ray diffraction (XRD) pattern

The crystalline structure and phase purity of both Fe_3O_4 and Fe_3O_4@CMI nanoparticles were confirmed by XRD, as shown in Fig. 2. All samples exhibited characteristic peaks corresponding to a single-phase cubic spinel structure (FCC), indicative of pure magnetite (JCPDS No. 19-0629; COD 9005841). The diffraction peaks observed at 2θ values of 18.3°, 30.2°, 35.6°, 37.2°, 43.3°, 53.7°, 57.2°, and 62.8° were indexed to the (111), (220), (311), (222), (400), (422), (511), and (440) planes, respectively. No additional peaks were detected, confirming the absence of secondary phases or impurities. The slight peak broadening and reduced intensity suggest nanoscale crystallite dimensions. Notably, the polymer coating did not alter the crystalline structure of Fe_3O_4, indicating that surface modification with CMI preserved the core magnetite phase.

3.1.2. Transmission electron microscopy (TEM) and particle size analysis

The TEM images of Fe_3O_4@CMI nanoparticles (Fig. 3a) show quasi-spherical particles with noticeable aggregation, which is typical for magnetic nanoparticles due to dipole–dipole interactions. The particles appear relatively uniform in size, with no significant morphological distortion after coating.

The particle size distribution (Fig. 3b) reveals an average diameter of 13 ± 2 nm, confirming the formation of nanoscale particles with a narrow size distribution. The relatively small size and uniformity are beneficial for enhancing surface area and interaction with scaling ions. The absence of significant size enlargement suggests that the CMI coating forms a thin organic layer that does not substantially alter the core dimensions.

3.1.3. Fourier Transform Infrared (FTIR) analysis

FTIR spectroscopy was used to confirm the successful coating of Fe_3O_4 with CMI, as shown in Fig. 4. The spectrum of pure CMI exhibited a broad band around 3290 cm^{-1}, attributed to O–H stretching vibrations from hydroxyl groups in the fructose and glucose units of the inulin backbone (Bernal et al., 2005; Ibrahim et al., 2006). Peaks near 2919 cm^{-1} corresponded to C–H stretching vibrations of aliphatic groups. The strong band at 1600 cm^{-1} was assigned to asymmetric stretching of carboxylate ($–COO^-$) groups, while additional peaks between 1400 and 1320 cm^{-1} were related to carbohydrate deformation modes such as –OCH and –COH (Ibrahim et al., 2006; Szarek et al., 1984). The region between 1200 and 1000 cm^{-1} contained signals for C–O, C–C–C, and C–O–C stretches, characteristic of polysaccharides. Specifically, the peak at 1009 cm^{-1} was associated with C–O stretching and H–C–O bending vibrations of hydroxymethyl groups. A distinct band at 916 cm^{-1}, attributed to C–CO deformation and –CO stretching, was also present (Rahul et al., 2014; Smith, 1979). These features were

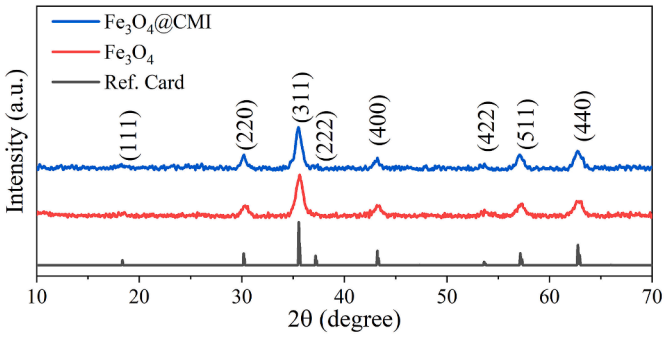

Fig. 2. XRD patterns of bare Fe_3O_4, Fe_3O_4@CMI nanoparticles, and reference for pure magnetite (JCPDS No. 19-0629).

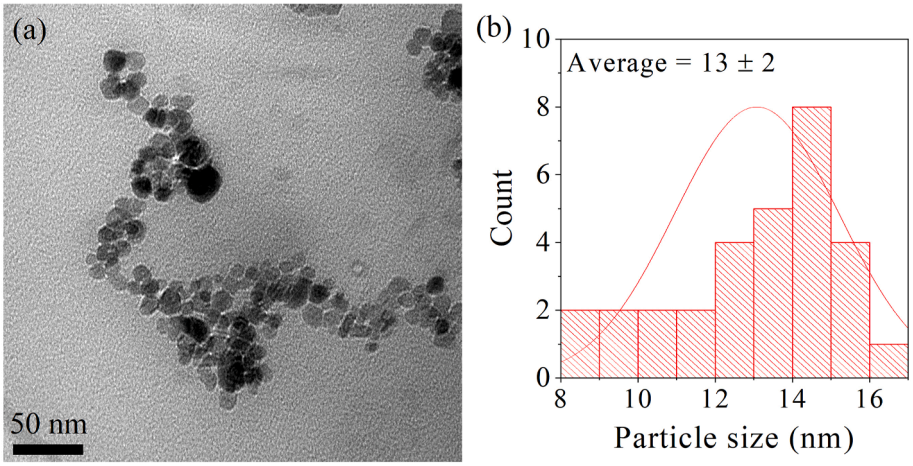

Fig. 3. (a) Transmission electron microscopy (TEM) image of Fe_3O_4@CMI nanoparticles. (b) Particle size distribution histogram of Fe_3O_4@CMI nanoparticles.

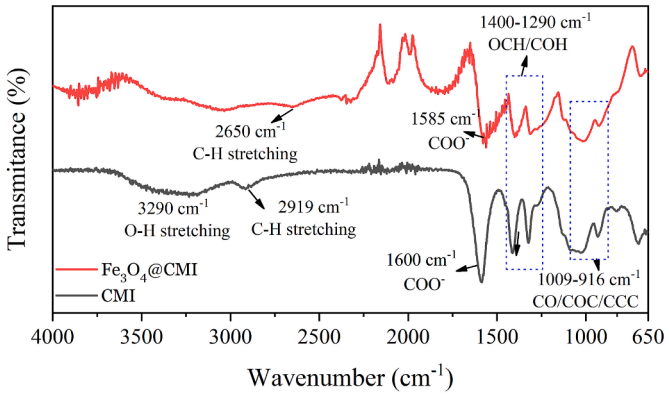

Fig. 4. FTIR spectra of pure CMI and Fe_3O_4@CMI nanoparticles.

retained in the Fe_3O_4@CMI spectrum, with slight shifts and broadening, indicating successful surface functionalization. The presence of absorption bands between 1585 and 916 cm^{-1} further confirmed the binding of CMI's carboxylate groups to the Fe_3O_4 surface.

3.1.4. Thermogravimetric Analysis (TGA)

TGA was performed to estimate the coating percentage of CMI on the MNPs (Fig. 5). Bare Fe_3O_4 showed minimal weight loss, primarily due to surface-adsorbed moisture. In contrast, pure CMI exhibited three distinct weight loss stages: the first between 25 and 200 °C, attributed to moisture evaporation; the second from 200 to 450 °C, corresponding to the decomposition of the inulin backbone; and the third between 450 and 650 °C, linked to the degradation of carboxymethyl groups and complete combustion of the organic material. The Fe_3O_4@CMI sample showed a similar thermal profile to that of CMI, confirming the successful surface coating. From the weight loss data, the coating percentage was estimated to be approximately 59 wt%, indicating a substantial polymer layer on the nanoparticle surface. These findings confirm effective surface modification.

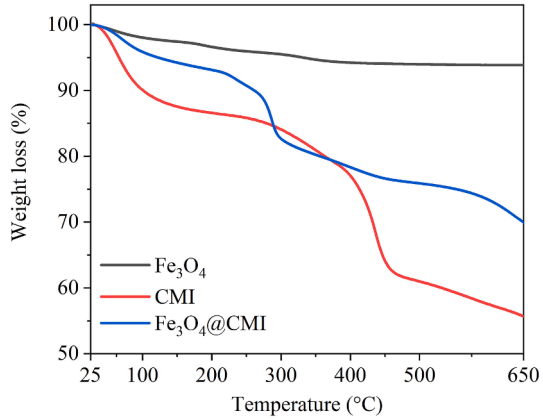

Fig. 5. TGA curves of bare Fe_3O_4, pure CMI, and Fe_3O_4@CMI nanoparticles.

3.1.5. Magnetometry

The magnetic behaviour of bare Fe_3O_4 and Fe_3O_4@CMI nanoparticles was characterized at room temperature (300 K), as shown in Fig. 6 and summarized in Table 1. Both samples exhibited negligible coercivity (Hc) and remanence (Mr), confirming superparamagnetic behaviour, which is a critical property for preventing particle agglomeration and fouling in flow systems (Min et al., 2020). The saturation magnetization (Ms) of bare Fe_3O_4 was 66.79 emu/g, while Fe_3O_4@CMI showed a reduced Ms of 46.63 emu/g due to the non-magnetic organic coating. Despite this decrease, the coated nanoparticles retained sufficient magnetic response for rapid separation using a permanent magnet. These results demonstrate that CMI functionalization preserves the desirable superparamagnetic properties of Fe_3O_4, enabling efficient dispersion in aqueous environments and magnetic recovery for reuse.

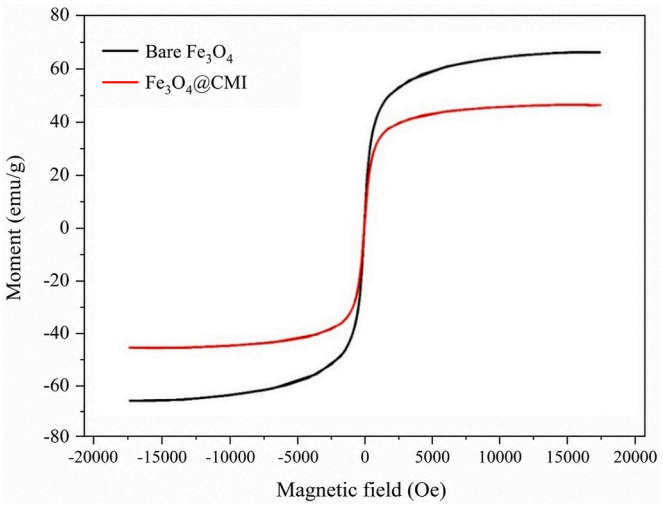

Fig. 6. Magnetic hysteresis loops of bare Fe_3O_4 and Fe_3O_4@CMI nanoparticles at 300 K.

Table 1
Magnetic properties of bare Fe_3O_4 and Fe_3O_4@CMI nanoparticles at room temperature.

Compound	Ms (emu/g)	Hc (Oe)	Mr (emu/g)
Bare Fe_3O_4	66.787	5.9003	0.54472
Fe_3O_4@CMI	46.632	6.4534	0.41651

3.2. Evaluation of the performance of Fe_3O_4@CMI SI

3.2.1. Static jar tests

The static scale inhibition performance of Fe_3O_4@CMI was evaluated against gypsum and calcite scales and compared to that of pure CMI (Table 2). Both inhibitors achieved 100% inhibition for both types of scale at 100 and 50 ppm. This behavior is attributed to the CMI coating, which introduces carboxylate groups (–COO^-) on the nanoparticle surface, enhancing interaction with scale-forming ions (e.g., Ca^{2+}) through electrostatic attraction and complexation. This facilitates adsorption at the crystal interface, thereby disrupting nucleation and crystal growth. At lower concentrations, this effect becomes more dependent on the availability of active sites, leading to observable differences in inhibition performance. Fe_3O_4@CMI maintained full inhibition for gypsum down to 5 ppm and still exhibited 95% inhibition at 1 ppm, indicating excellent performance. For calcite, however, inhibition efficiency dropped more noticeably, with only 17% inhibition observed at both 2 and 1 ppm. In comparison, pure CMI showed consistently higher performance at lower concentrations for calcite, retaining 55% inhibition even at 1 ppm. The reduced efficiency of Fe_3O_4@CMI at low concentrations, particularly for calcite, may be attributed to limited surface availability of active sites due to partial coverage of the polymer on the nanoparticle surface (around 59 wt% polymer coating, providing the active inhibition sites) alongside the contribution of some of CMI in attaching to the MNPs, so they don't participate in the inhibition process. Nevertheless, the coated inhibitor demonstrated excellent performance at moderate to high concentrations, especially for gypsum, highlighting its potential as a robust scale control agent under static conditions.

3.2.2. Reusability assessment

The reusability of Fe_3O_4@CMI was evaluated over five cycles using static jar tests at a constant concentration of 100 ppm (Table 3). For gypsum scale, the coated nanoparticles consistently maintained 100% inhibition through the first three reuse cycles, with only a slight decrease to 96% and 95% in the fourth and fifth cycles, respectively. In contrast, calcite inhibition declined more rapidly, dropping to 82% in the first reuse and down to 30% by the fourth cycle. To understand the reasons, we should consider the following: as highlighted in Table 2, gypsum inhibition requires significantly lower effective concentrations (5 ppm) than calcite (50 ppm), so the Fe_3O_4@CMI SI is still effective to inhibit gypsum, but is not for the calcite. The observed decline in calcite inhibition may reflect the surface deactivation, or in other words, the accumulation of calcite crystals during recovery and washing steps on active spots of the SI surface, leading to participation of these crystals as nucleation sites for additional calcite scales. Nevertheless, the SI composite demonstrates promising recyclability potential, especially for sulfate-based scales.

Table 2
Static jar test results showing inhibition efficiencies of pure CMI and Fe_3O_4@CMI against gypsum and calcite scales at various concentrations.

SI concentration (ppm)	% inhibition at a given dosage (±5%)			
	Pure CMI		Fe_3O_4@CMI (59% active)	
	Gypsum	Calcite	Gypsum	Calcite
100	100	100	100	100
50	100	100	100	100
20	100	100	100	83
10	100	73	100	67
5	100	73	100	50
2	100	73	97	17
1	100	55	95	17

Table 3
Reusability performance of Fe_3O_4@CMI (100 ppm) against gypsum and calcite.

Number of recycling Fe_3O_4@CMI SI at (100 ppm)	Inhibition (±5%)	
	Gypsum	Calcite
0 (original)	100	100
1	100	82
2	100	63
3	100	47
4	96	30
5	95	-

To further assess the integrity of the coating during reuse, FTIR analysis was performed on the supernatant after magnetic separation as well as on the recovered Fe_3O_4@CMI after the 5th cycle (Fig. S2). No characteristic CMI peaks were detected in the supernatant, confirming negligible polymer leaching into the bulk solution. In addition, the FTIR spectra of the recovered material remained unchanged, indicating preservation of the CMI coating. These findings support that the observed inhibition performance is primarily governed by interfacial interactions of the coated nanoparticles rather than free inhibitor in solution.

3.2.3. SEM measurement

Fig. 7 shows the surface morphology of the coated magnetite scale inhibitor (Fe_3O_4@CMI SI) after the first inhibition run at two concentrations: 10 ppm and 100 ppm. At 10 ppm, Fe_3O_4@CMI SI demonstrated full inhibition of the gypsum scale, with comparable results observed at 100 ppm (Fig. 7a and b). For calcite and barite, the scale crystals formed in the presence of 10 ppm Fe_3O_4@CMI SI exhibited rhombohedral and orthorhombic morphologies, respectively (Fig. 7c and e). However, increasing the concentration to 100 ppm led to a clear transformation of these structures into irregular, non-uniform forms (Fig. 7d and f), with visible inhibitory material coating the scale surfaces. These morphological disruptions confirm the inhibitor's strong interaction with scale-forming ions, especially under higher-dose conditions. The SEM findings support the inhibition trends observed in performance tests, highlighting Fe_3O_4@CMI's effectiveness in disrupting crystal growth and altering scale habit.

3.2.4. Calcium compatibility

Calcium compatibility tests were conducted to assess the stability of Fe_3O_4@CMI in high-salinity environments containing calcium ions (Ca^{2+}), simulating field-like brine conditions. As shown in Tables 4 and 5, no turbidity or precipitation was observed at any concentration or time point (30 min, 1 h, 4 h, and 24 h), indicating excellent compatibility. A parallel test with pure CMI showed good compatibility with Ca^{2+} ions up to a concentration of 10000 ppm of SI after mixing. However, it began to exhibit haziness after 1 h, leading to precipitation for the remainder of the test, as shown in Tables S3 and S4. These results confirm that Fe_3O_4@CMI enhances the compatibility of CMI with Ca^{2+} ions, remains stable in the presence of high calcium concentrations, and does not induce secondary precipitation, which is critical for preventing formation damage during oilfield applications.

3.2.5. High-pressure dynamic tube blocking tests

The dynamic performance of Fe_3O_4@CMI SI for gypsum, calcite, and barite scales was evaluated under HPHT conditions using a tube blocking rig, with results summarized in Table 6 and Fig. 8. The inhibitor was tested at concentrations of 1, 2, 5, 10, 20, 50, and 100 ppm, in addition to a blank (0 ppm). It should be noted that complete inhibition (no pressure increase) was observed at higher concentrations, while this table reports the first concentration at which scale formation occurred.

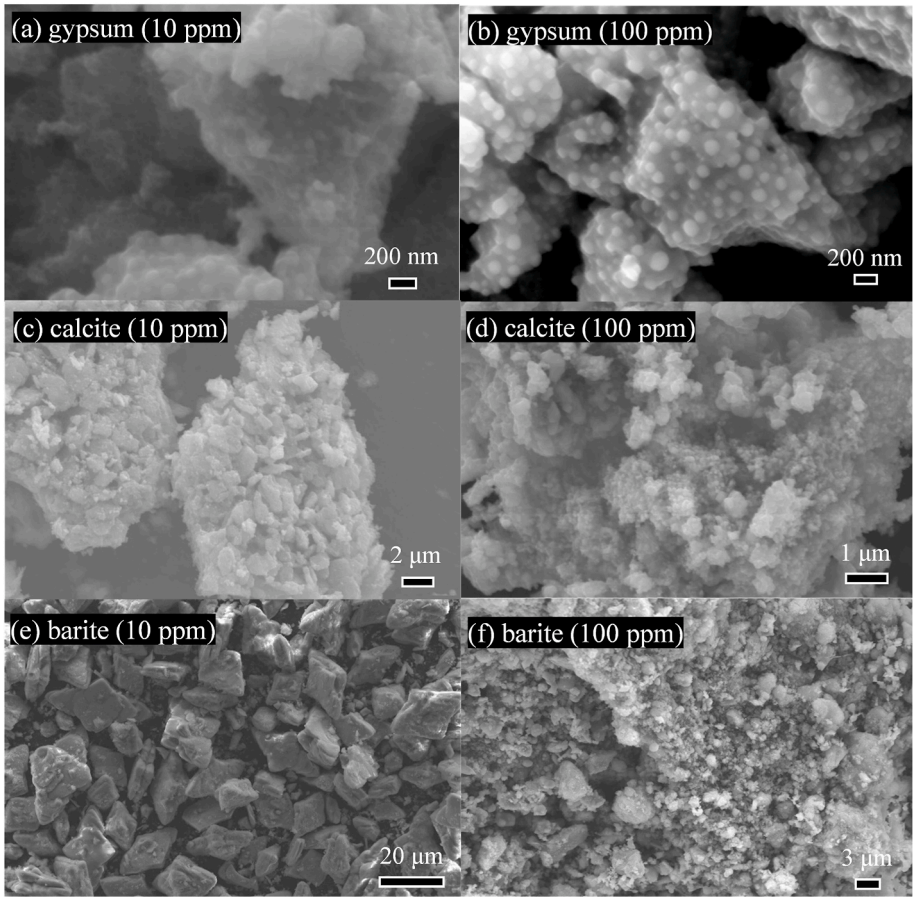

Fig. 7. SEM images of gypsum, calcite, and barite scale deposits formed in the presence of Fe_3O_4@CMI at 10 ppm (a, c, e) and 100 ppm (b, d, f).

For gypsum scale, the blank test showed pressure buildup within 26 min, indicating rapid scale formation. At 2 ppm, Fe_3O_4@CMI delayed gypsum scaling, maintaining performance for 32 min. This indicates that complete inhibition was achieved at higher concentrations (≥5 ppm). In comparison, pure CMI achieved complete inhibition at the same concentrations. For calcite, scale formation occurred rapidly in the blank test, with blockage observed within 8 min. Fe_3O_4@CMI showed complete inhibition at higher concentrations (≥50 ppm), while at 20 ppm, partial scaling occurred within 7 min, indicating insufficient inhibition at lower dosage. In contrast, pure CMI maintained effective inhibition at significantly lower concentrations, fully preventing scale at just 5 ppm. A similar trend was observed for barite. While Fe_3O_4@CMI achieved complete inhibition at higher concentrations (≥50 ppm), partial scaling was observed at 20 ppm. Pure CMI demonstrated higher efficiency, remaining effective at 10 ppm. Based on the dynamic test results, the optimal dosage of Fe_3O_4@CMI was found to be scale-dependent, with complete inhibition achieved at ≥5 ppm for gypsum and ≥50 ppm for calcite and barite under HPHT flow conditions.

These results highlight that Fe_3O_4@CMI required higher dosages under dynamic conditions relative to pure CMI, particularly for calcite and barite. This performance difference aligns with static test results (Table 2), where 50 ppm of Fe_3O_4@CMI was needed to achieve complete inhibition of calcite, compared to 20 ppm for pure CMI. However, the gap between inhibitors is more pronounced under dynamic conditions, where the failure inhibitor concentration (FIC) for Fe_3O_4@CMI rose to 20 ppm, versus just 5 ppm for CMI. This can be attributed to differences in scale formation kinetics and polymer–scale interactions under HPHT conditions (Al-Roomi & Hussain, 2016; Jafar Mazumder, 2020; Kelland, 2016). In addition, only ~59 wt% of Fe_3O_4@CMI corresponds to the CMI coating, which represents the active inhibitory component, while the remaining Fe_3O_4 core primarily provides magnetic functionality. This reduces the effective concentration of active inhibitor in the system. In addition, immobilization of CMI onto the nanoparticle surface may limit the accessibility and mobility of some functional groups compared to free CMI in solution. This restriction can reduce the efficiency of interaction with scale-forming ions, particularly under dynamic flow conditions where rapid transport to nucleation sites is required. Furthermore, the relatively high polymer content (~59 wt%) may lead to partial shielding or reduced accessibility of active sites after immobilization, further contributing to the lower inhibition efficiency compared to pure CMI. The lower performance under dynamic conditions may also be influenced by mass transfer limitations, as the larger nanoparticle system is less mobile than dissolved inhibitor molecules, reducing the rate at which active sites reach crystal nucleation points on the tube wall (Kamal et al., 2018). These results indicate that although Fe_3O_4@CMI required slightly higher doses to match the inhibition efficiency of pure CMI under dynamic flow, its calcium compatibility and magnetic recoverability provide practical advantages in long-term field applications.

The performance of Fe_3O_4@CMI was further compared with conventional oilfield scale inhibitors such as phosphonates and polymeric systems. These inhibitors are typically effective at low concentrations in the range of 1–50 ppm, depending on system conditions (Mpelwa & Tang, 2019). In comparison, Fe_3O_4@CMI demonstrated effective inhibition at ≥5 ppm for gypsum and ≥50 ppm for calcite and barite, indicating competitive performance within this range. In addition, its magnetic recoverability and reusability provide practical advantages for field applications.

Although higher minimum inhibitor concentrations are required for certain scales, this trade-off is partially offset by the magnetic

Table 4
Visual assessment of calcium compatibility for Fe_3O_4@CMI at varying Ca^{2+} and inhibitor concentrations after 24 h of incubation at 80 °C.

Ca^{2+} dose (ppm)	SI dose (ppm)			SI dose (ppm) after collecting MNPs		
	100	1000	10000	10000	1000	100
100	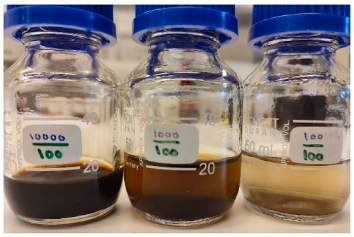			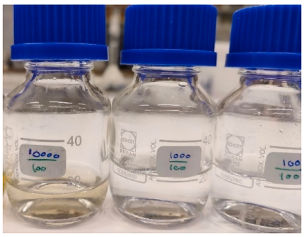		
1000	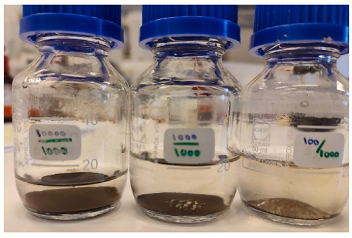			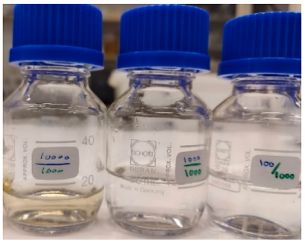		
10000	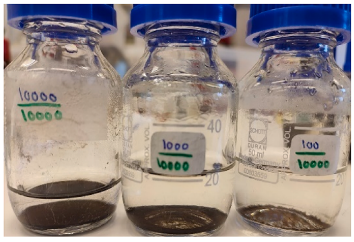			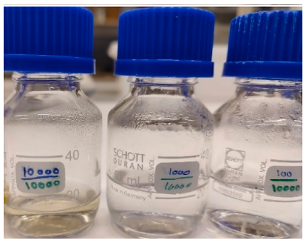		

Table 5
Time-resolved compatibility results for Fe_3O_4@CMI with Ca^{2+} in 3 wt% NaCl solution, monitored at 30 min, 1 h, 4 h, and 24 h at 80 °C.

Ca^{2+} dose (ppm)	Fe_3O_4@CMI SI dose (ppm)	Appearance				
		After mixing	30 min	1 h	4 h	24 h
100	100	clear	clear	clear	clear	clear
	1000	clear	clear	clear	clear	clear
	10000	clear	clear	clear	clear	clear
1000	100	clear	clear	clear	clear	clear
	1000	clear	clear	clear	clear	clear
	10000	clear	clear	clear	clear	clear
10000	100	clear	clear	clear	clear	clear
	1000	clear	clear	clear	clear	clear
	10000	clear	clear	clear	clear	clear

recoverability and reusability of the nanocomposite, which can reduce overall chemical consumption over multiple cycles. In addition, the enhanced calcium compatibility minimizes the risk of secondary precipitation, improving operational reliability in high-salinity environments.

4. Conclusion

This study demonstrates the potential of Fe_3O_4@CMI nanoparticles as a recyclable scale inhibitor for oilfield applications. The synthesized Fe_3O_4@CMI nanocomposite exhibited strong scale inhibition performance under both static and dynamic conditions, particularly against gypsum. In static tests, full inhibition of gypsum was maintained even at very low concentrations, while dynamic tests confirmed its effectiveness for gypsum, calcite, and barite under high-pressure conditions. Although slightly higher doses were required compared to pure CMI, Fe_3O_4@CMI offered the added advantage of magnetic properties for recovery and reuse, as well as enhanced calcium compatibility. Reusability assessments showed consistent gypsum inhibition over multiple cycles, with minimal performance loss. Calcite inhibition-maintained half of its inhibition after 3 cycles, which is considered a good result for a harsher scale. The Fe_3O_4@CMI SI provides a significant advantage in sustainability by enhancing calcium compatibility, reducing chemical discharge, and enabling some magnetic recovery. These results highlight the material's promise as a recyclable alternative for scale control in oilfield operations, particularly in applications that prioritize reusability and environmental safety.

Table 6
Summary of dynamic tube blocking test results for gypsum, calcite, and barite scales. Times represent the duration before scale formation occurred, with and without inhibitors, at various concentrations.

Scale	Scale inhibitor	1st blank	First scale test		Second scale test		2nd blank
		Time (mins)	Conc. (ppm)	Time (mins)	Conc. (ppm)	Time (mins)	Time (mins)
Gypsum	Fe_3O_4@CMI	26	2	32	2	22	28
	Pure CMI	29	No scale	-	No scale	-	30
Calcite	Fe_3O_4@CMI	8	20	7	20	6	7
	Pure CMI	8	5	3	5	11	8
Barite	Fe_3O_4@CMI	7	20	10	20	8	7
	Pure CMI	8	10	14	10	15	9

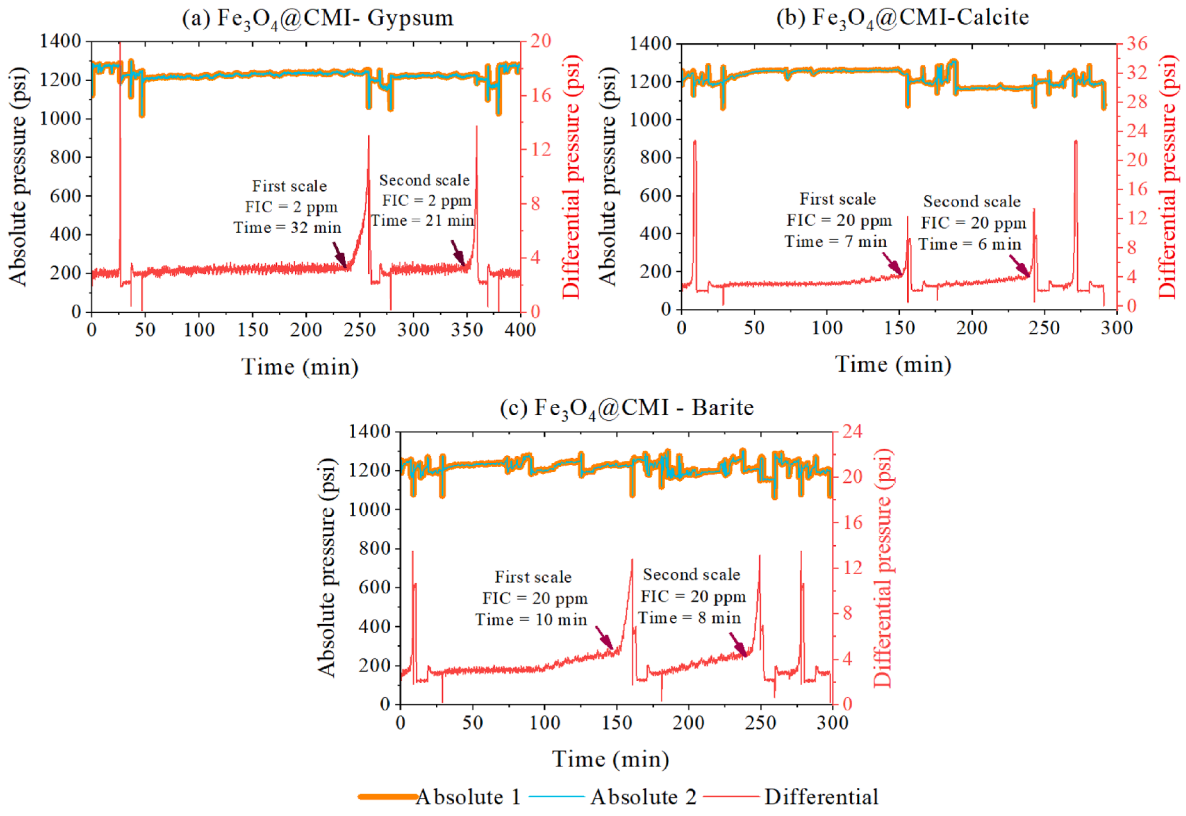

Fig. 8. Pressure profiles during dynamic scale inhibition tests using Fe_3O_4@CMI against (a) gypsum, (b) calcite, and (c) barite scales. Stable pressure indicates successful inhibition, while a sharp increase denotes scale deposition.

CRediT authorship contribution statement

Abdelrahman T. Abdelaal: Writing – original draft, Methodology. **Farah M. El-Makaty:** Writing – original draft. **Malcolm A. Kelland:** Writing – review & editing, Supervision. **Mohamed F. Mady:** Writing – review & editing, Validation, Supervision, Resources, Project administration, Funding acquisition, Formal analysis, Conceptualization.

Declaration of competing interest

The authors declare that they have no known competing financial interests or personal relationships that could have appeared to influence the work reported in this paper.

Acknowledgements

We thank the Research Council of Norway for the financial support of the Ph.D. Candidate Abdelrahman Abdelaal, through the project PETROMAKS 2 programme/Research Project No. 300754. This work was supported by Grant no. ARG01-0602-230467 from Qatar National Research Fund (a member of the Qatar Foundation). Open access publication of this article is funded by the Qatar National Library.

Appendix A. Supplementary data

Supplementary data to this article can be found online at https://doi.org/10.1016/j.partic.2026.05.004.

References

Abdelaal, A. T., Kelland, M. A., Castro, D. L. Q., & Mady, M. F. (2024). Nano-engineered Polyaspartate-Coated magnetite scale inhibitor: A sustainable solution for efficient gypsum scale control in oilfield operations. *ACS Appl. Eng. Mater., 2*(4), 1131–1140.

Al-Roomi, Y. M., & Hussain, K. F. (2016). Potential kinetic model for scaling and scale inhibition mechanism. *Desalination, 393*, 186–195.

Bernal, B. H., Calle, J., Duarte, E. Q., Pinzón, R., & Velásquez, M. (2005). Inulina a partir de tubérculos de Dahlia imperialis Roetz. *Revista Colombiana de Ciencias Químico Farmacéuticas*, 122–125.

Boels, L., & Witkamp, G.-J. (2011). Carboxymethyl inulin biopolymers: A green alternative for phosphonate calcium carbonate growth inhibitors. *Crystal Growth & Design, 11*(9), 4155–4165.

Boumagoura, M., Ghizellaoui, S., Rhouati, S., Cheap-Charpentier, H., & Horner, O. (2021). Calcium carbonate scaling prevention by a green chemical inhibitor, gallic acid. *Water and Environment Journal, 35*(3), 998–1006.

Chauhan, K., Sharma, P., & Chauhan, G. S. (2015). Chapter 29: Removal/dissolution of mineral scale deposits. *Mineral Scales and Deposits*, 701–720.

Chen, J., Chen, F., Han, J., Su, M., & Li, Y. (2020). Evaluation of scale and corrosion inhibition of modified polyaspartic acid. *Chemical Engineering & Technology, 43*(6), 1048–1058.

Cornell, R. M., & Schwertmann, U. (2003). *The iron oxides: Structure, properties, reactions, occurrences, and uses* (Vol. 664). Wiley-vch Weinheim.

Cullity, B. (1972). *Introduction to magnetic materials*. New Jersey: Addison-Wiley Publishing Company, 1972.

Dias, A. M. G. C., Hussain, A., Marcos, A. S., & Roque, A. C. A. (2011). A biotechnological perspective on the application of iron oxide magnetic colloids modified with polysaccharides. *Biotechnology Advances, 29*(1), 142–155.

F Hasany, S., H Abdurahman, N., R Sunarti, A., & Jose, R. (2013). Magnetic iron oxide nanoparticles: Chemical synthesis and applications review. *Current Nanoscience, 9*(5), 561–575.

Frenier, W. W.; Ziauddin, M., Formation, removal, and inhibition of inorganic scale in the oilfield environment. Society of Petroleum Engineers.

Guo, X., Qiu, F., Dong, K., Zhou, X., Qi, J., Zhou, Y., & Yang, D. (2012). Preparation, characterization and scale performance of scale inhibitor copolymer modification with chitosan. *Journal of Industrial and Engineering Chemistry, 18*(6), 2177–2183.

Häfeli, U., Schütt, W., Teller, J., & Zborowski, M. (2013). *Scientific and clinical applications of magnetic carriers*. Springer Science & Business Media.

Hasson, D., Shemer, H., & Sher, A. (2011). State of the art of friendly "green" scale control inhibitors: A review article. *Industrial & Engineering Chemistry Research, 50*(12), 7601–7607.

Ibrahim, M., Alaam, M., El-Haes, H., Jalbout, A. F., & Leon, A.d. (2006). Analysis of the structure and vibrational spectra of glucose and fructose. *Ecletica quimica, 31*, 15–21.

Jafar Mazumder, M. A. (2020). A review of green scale inhibitors: Process, types, mechanism and properties. *Coatings, 10*(10), 928.

Johannsen, F. R. (2003). Toxicological profile of carboxymethyl inulin. *Food and Chemical Toxicology, 41*(1), 49–59.

Kamal, M. S., Hussein, I., Mahmoud, M., Sultan, A. S., & Saad, M. A. S. (2018). Oilfield scale formation and chemical removal: A review. *Journal of Petroleum Science and Engineering, 171*, 127–139.
Kelland, M. A. (2016). *Production chemicals for the oil and gas industry*. CRC press.
Kirboga, S., & Öner, M. (2013). Investigation of calcium carbonate precipitation in the presence of carboxymethyl inulin. *CrystEngComm, 15*(18), 3678–3686.
Kodel, K. A., Andrade, P. F., Valença, J. V. B., & Souza, D.d. N. (2012). Study on the composition of mineral scales in oil Wells. *Journal of Petroleum Science and Engineering, 81*, 1–6.
Kumar, S., Naiya, T. K., & Kumar, T. (2018). Developments in oilfield scale handling towards green technology-A review. *Journal of Petroleum Science and Engineering, 169*, 428–444.
Liu, X., Chen, T., Chen, P., Montgomerie, H., Hagen, T., Wang, B., & Yang, X. (2012). Understanding mechanisms of scale inhibition using newly developed test method and developing synergistic combined scale inhibitors. In *SPE international conference on oilfield scale*. OnePetro.
Lu, A.-H., Salabas, E. L., & Schüth, F. (2007). Magnetic nanoparticles: Synthesis, protection, functionalization, and application. *Angewandte Chemie International Edition, 46*(8), 1222–1244.
Mady, M. F. (2022). Chapter 16 - Oilfield scale inhibitors: Synthetic and performance aspects. In Z. Amjad, & K. D. Demadis (Eds.), *Water-formed deposits* (pp. 325–352). Elsevier.
Mady, M. F., Bayat, P., & Kelland, M. A. (2020). Environmentally friendly phosphonated polyetheramine scale inhibitors—excellent calcium compatibility for oilfield applications. *Industrial & Engineering Chemistry Research, 59*(21), 9808–9818.
Mady, M. F., Karaly, A. H., & Kelland, M. A. (2023). Phosphonated polyetheramine-coated superparamagnetic iron oxide nanoparticles for inhibition of oilfield scale. *ACS Applied Nano Materials*.
Mady, M. F., Rehman, A., & Kelland, M. A. (2021). Synthesis and study of modified polyaspartic acid coupled phosphonate and sulfonate moieties as green oilfield scale inhibitors. *Industrial & Engineering Chemistry Research, 60*(23), 8331–8339.
Min, J., Kang, D. W., Ahn, Y.-H., Lee, W., Cha, M., & Lee, J. W. (2020). Recoverable magnetic nanoparticles as hydrate inhibitors. *Chemical Engineering Journal, 389*, Article 124461.
Mpelwa, M., & Tang, S.-F. (2019). State of the art of synthetic threshold scale inhibitors for mineral scaling in the petroleum industry: A review. *Petroleum Science, 16*(4), 830–849.
Oshchepkov, M., Golovesov, V., Ryabova, A., Frolova, S., Tkachenko, S., Kamagurov, S., Rudakova, G., & Popov, K. (2020). Synthesis and visualization of a novel fluorescent-tagged polymeric antiscalant during gypsum crystallization in combination with bisphosphonate fluorophore. *Crystals, 10*(11), 992.
Popov, K. I., Kovaleva, N. E., Rudakova, G. Y., Kombarova, S. P., & Larchenko, V. E. (2016). Recent state-of-the-art of biodegradable scale inhibitors for cooling-water treatment applications. *Thermal Engineering, 63*(2), 122–129 (Review).
Rahul, R., Jha, U., Sen, G., & Mishra, S. (2014). Carboxymethyl inulin: A novel flocculant for wastewater treatment. *International Journal of Biological Macromolecules, 63*, 1–7.
Salman, A. D., Alardhi, S. M., AlZubaidi, A. A. H., AlJaberi, F. Y., Zsirka, B., Nhat, T., Jakab, M., Borsfai, R., Ali, O. I., & Le, P. C. (2026). Novel EDTA-Modified Santa Barbara Amorphous-15 and Fe3O4@SiO2 adsorbents for highly efficient Ni (II) removal from aqueous solutions. *International Journal of Environmental Science and Technology, 23*(3), 202.
Salman, D., Juzsakova, T., Al-Mayyahi, M. A., Ákos, R., Mohsen, S., Ibrahim, R. I., Mohammed, H. D., Abdullah, T. A., Domokos, E., & Korim, T. (2021). Synthesis, surface modification and characterization of magnetic Fe3O4@SiO2 core-shell nanoparticles. *Journal of Physics: Conference Series, 1773*(1), Article 012039.
Santiago-Rodríguez, L., Lafontaine, M. M., Castro, C., Méndez-Vega, J., Latorre-Esteves, M., Juan, E. J., Mora, E., Torres-Lugo, M., & Rinaldi, C. (2013). Synthesis, stability, cellular uptake, and blood circulation time of carboxymethyl-inulin coated magnetic nanoparticles. *Journal of Materials Chemistry B, 1*(22), 2807–2817.
Smith, A. L. (1979). Applied infrared spectroscopy. Fundamentals, techniques and analytical problem solving. *Applied infrared spectroscopy. Fundamentals*.
Szarek, W. A., Korppi-Tommola, S.-L., Shurvell, H. F., Smith Jr, V. H., & Martin, O. R. (1984). A Raman and infrared study of crystalline D-fructose, L-sorbose, and related carbohydrates. Hydrogen bonding and sweetness. *Canadian Journal of Chemistry, 62*(8), 1512–1518.
Tm, N. S. (2007). Laboratory screening tests to determine the ability of scale inhibitors to prevent the precipitation of calcium sulfate and calcium carbonate from solution (for oil and gas production systems). *National Association of Corrosion Engineers*, 2007.
Wang, H., Yang, J., Fang, C., Li, C., Zhong, G., & Peng, C. (2020). Synthesis and characterization of modified sodium carboxymethyl cellulose and polyethylene glycol ester new copolymer as scale inhibitor. *Desalination and Water Treatment, 191*, 285–291.
Wei, L., Lin, Y., Li, C., Wang, S., Gong, C., Jiang, Y., & Li, Z. (2022). Performance and mechanism study of PESA-IA as a green oilfield scale inhibitor: Experimental and molecular dynamics simulation. *Journal of Polymer Research, 29*(12), 1–11.
Wu, W., He, Q., & Jiang, C. (2008). Magnetic iron oxide nanoparticles: Synthesis and surface functionalization strategies. *Nanoscale Research Letters, 3*(11), 397.
Zhang, Y., Yin, H., Zhang, Q., Li, Y., Yao, P., & Huo, H. (2018). A novel polyaspartic acid derivative with multifunctional groups for scale inhibition application. *Environmental Technology, 39*(7), 843–850.